Available online at www.sciencedirect.com
ScienceDirect
Journal of Sound and Vibration 324 (2009) 850–860
JOURNAL OF SOUND AND VIBRATION
www.elsevier.com/locate/jsvi

New graphical techniques for studying acoustic ray stability

T. Bódai[a], A.J. Fenwick[b,a], M. Wiercigroch[a,*]

[a]*Centre for Applied Dynamics Research, School of Engineering, Kings College, University of Aberdeen, Aberdeen, AB24 3UE, UK*
[b]*QinetiQ, Cody Technology Park, Farnborough, GU14 0LX, UK*

Received 15 February 2008; received in revised form 13 January 2009; accepted 28 January 2009
Handling Editor: C.L. Morfey
Available online 14 March 2009

Abstract

Alternatives to the standard Poincaré section are proposed to cater for some conditions arising in the study of chaotic ray propagation where the usual method of dimension reduction by the Poincaré section is inadequate because the driving is not periodic. There are three alternatives proposed which all use the same surface of intersection, but which differ in their use of the values of the dependent variables at the intersections of the rays with the surface. The new reduction techniques are used to examine ray behaviour in a harmonically perturbed Munk profile which supports ray chaos. It is found that all three techniques provide a graphical means of distinguishing between regular and irregular motions, and that the space of the mapping associated with one of them is partitioned into nonintersecting regular and chaotic regions as with the Poincaré section. A further model with quasiperiodic time dependence of the Hamiltonian is examined, and it turns out that the quasiperiodic nature of the motion is revealed as Lissajous curves by one technique.

1. Introduction

This paper is concerned with the study of long range ducted sound propagation in a deep ocean, which is relevant for many practical applications. For example, underwater acoustic propagation has been extremely important in predicting the performance of military sonar systems for several decades. For almost as long, and increasingly so over the last 20 years, acoustic systems have been used for environmental and climatological studies. One of these is the measurement of the average speed of sound over long range as indicator of global warming, since the speed of sound is dependent on temperature. Communication and navigation are other applications and an understanding of long range propagation is required in systems studies, an interesting example being to define an infrastructure for integrated ocean observatories and navigation beacons.

The propagation of sound can be modelled approximately but to sufficient accuracy, using differential equations for the ray paths which describe the geometrical optics approximation. The equations are developed from the paraxial approximation to the acoustic wave equation and result in a parabolic equation valid for ray paths a few degrees from the horizontal [16]. The ray equations depend on the sound speed variation with position. Under the simplifying assumption that the ocean is layered, so that the sound speed depends only on

*Corresponding author.
E-mail address: m.wiercigroch@abdn.ac.uk (M. Wiercigroch).

0022-460X/$ - see front matter © 2009 Elsevier Ltd. All rights reserved.
doi:10.1016/j.jsv.2009.01.049

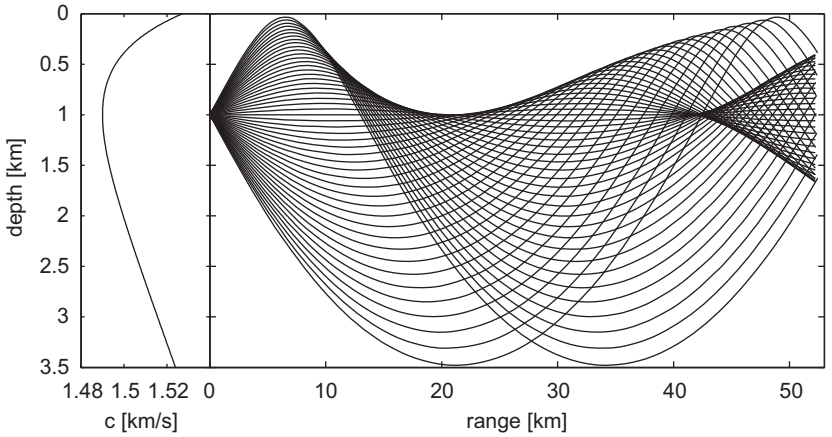

Fig. 1. Tunnelling ray paths (right panel) in a wave guide given by the canonical Munk profile (left panel and Eq. (7)). Initial conditions are: $z_0 = z_a$ and $\varphi_0 = \pm 1^\circ, 2^\circ, \ldots, 12^\circ$.

depth, the ray equations can be reduced to a system of two autonomous equations for the tangent of ray grazing angle and depth of a ray, with range as the independent variable. Fig. 1 shows a set of ray paths for one sound speed profile used to model the ambient conditions in the deep ocean.

When the layers are perturbed by a range dependent sound speed variation, the equations are modified to include a driving term and under suitable conditions [3], chaos can result. The effect of this on travel time was extensively studied by Smirnov et al. [13–15]. Ray chaos gives a reasonable account for various features of wave propagation observed in data collected during long range sound transmission experiments [1].

If ray chaos occurs, it implies that the acoustic field at a point beyond ray chaos is fully developed cannot be predicted by ray-based theories. Assessing when it may occur is, therefore, an important issue. Ray chaos occurs when the ray paths are unstable and the study of ray stability in various ocean environments is the means to carry out the assessment. There are various numerical and geometrical tools, including those first proposed by Poincaré, the Poincaré return map or the Poincaré section. This paper proposes further reduction techniques as tools for geometrical investigations of ray stability.

First, the mathematical theory of ray propagation in a layered ocean is described and a simple model for a harmonic sound speed perturbation is introduced. Ray stability in this model is investigated using the Poincaré section method. An alternative model for background profile and periodic sound speed perturbation is cited along with an alternative to the Poincaré return map more suited to this case, which is then applied to the above introduced model. Three other graphical representations of propagation behaviour are then proposed for the case where the perturbation is not periodic. They are first applied to the harmonic perturbation example, and then a model with quasiperiodic perturbation is used to evaluate the third of the reduction techniques. In the last section, we discuss our results, and compare them with results of another approach.

2. Mathematical model

The results, in this paper, are based on a system of ray equations which is consistent with the standard parabolic wave equation, introduced into underwater acoustics by Hardin and Tappert [8]. The solution of the parabolic equation, ψ, is the envelope of the acoustic pressure of a constant frequency wave field. In a cylindrical coordinate system it is written as

$$2ik_0\partial_r\psi + \partial_{zz}\psi + k_0^2(n^2 - 1)\psi = 0. \tag{1}$$

The index of refraction, $n = c_0/c$ is generally a spatial function via the sound speed $c = c(r, z)$. The reference sound speed c_0 is an arbitrary constant. The reference wavenumber $k_0 = \omega/c_0$ involves ω, the angular

frequency of the wave field. Assuming the solution in form of a ray series,

$$\psi = e^{i\omega\tau}\sum_{j=0}^{\infty}\frac{A_j}{(i\omega)^j}, \tag{2}$$

and substituting it into (1), the corresponding eikonal (Hamilton–Jacobi) equation results by taking the terms of the leading order in ω [9]:

$$\partial_r\tau + \frac{c_0}{2}(\partial_z\tau)^2 + \frac{1-n^2}{2c_0} = 0. \tag{3}$$

The eikonal has the dimension of time, and gives the surfaces of equal phase during propagation. It is also often referred to as 'travel time' or 'time-of-flight'. It can be shown that the solution of the Hamilton–Jacobi equation can be reduced to solving a Hamiltonian set of ordinary differential equations. Its canonical form for the pair of conjugate variables depth z and ray tangent p takes the form

$$z' = \partial_p\mathscr{H}, \quad p' = -\partial_z\mathscr{H}, \tag{4}$$

where the Hamiltonian of the ray system is

$$\mathscr{H}(r,z,p) = \frac{p^2}{2} + \frac{1-n^2}{2}. \tag{5}$$

The prime denotes differentiation with respect to range, the independent variable. The solution $z(r)$ is referred to as the ray path, and the $z-p$ trajectory as the ray trajectory. In plotting the trajectory, the ray tangent is replaced by the more intuitive variable, the ray angle: $\varphi = \arctan(p)$. The second term of the Hamiltonian is analogous to the potential function in mechanical systems. For calculations we use its linear approximation in terms of the normalised sound speed $C = n^{-1}$: $V = [1 - C^{-2}]/2 \approx C - 1$, which is obtained by a Taylor expansion about $C_0 = 1$, supposing small deviation of C from this value everywhere. With this, the ray equations can be detailed in the following way:

$$z' = p, \quad p' = -\partial_z C. \tag{6}$$

The canonical wave guide model. From Eq. (6), it is evident that C is required to specify the equations fully. Our first choice is the range independent Munk profile [11], shown in the left panel of Fig. 1, and described as

$$C(z) = c(z)/c_a = 1 + \varepsilon(\mathrm{e}^{-\eta(z)} + \eta(z) - 1), \quad \eta = 2(z - z_a)/B. \tag{7}$$

The minimum sound speed $c_a = c(z_a)$ is taken to be the reference sound speed. Following a common choice [12], we take $B = z_a = 1\,\mathrm{km}$, $c_a = 1.492\,\mathrm{km/s}$, $\varepsilon = 0.0057$. This profile has a minimum which creates a waveguide by confining the ray paths to tunnel around the sound channel axis. The waveguide feature of this ocean model is analogous to potential wells in mechanical systems. The Munk profile is range independent, so admits periodic ray paths like those in Fig. 1. These ray paths cross each other, and the wave fronts are said to be folded. Folding occurs more often at longer distances from the source.

3. Periodically perturbed wave guide

The Munk profile is the simplest realistic model of the deep ocean sound speed variation, being derived from equilibrium conditions for ambient oceanographic variables [11]. Variation in conditions can result in displacement of water particles due to a number of oceanographic effects. This produces a variation in sound speed known as internal wave. The fine structure of internal waves which is attributed to vertical water parcel displacement, the dominant contribution to small scale variability regarding acoustic ray stability, can be described by the Garrett–Munk spectrum [6]. Due to the small magnitudes and range scales, this variation is often referred to as a perturbation of the background structure.

A realistic model of the sound speed perturbation proposed in Ref. [5] involves up to 50 randomly phased modes with harmonic range dependency and some depth structure, consistent with the Garrett–Munk internal-wave spectrum [6]. A simple model from Ref. [17] takes an approximation for the first mode of

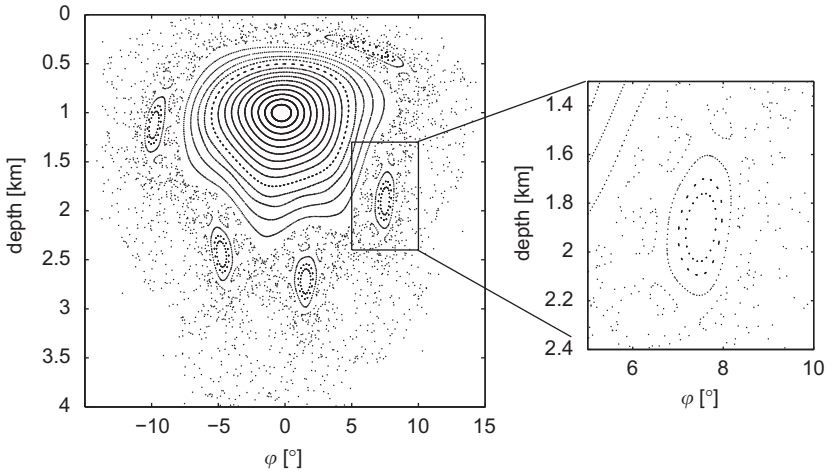

Fig. 2. Poincaré section of ray trajectories. Parameters of single mode perturbation are: $A = 0.01$ and $R = 10$ km. Initial conditions are: $z_0 = z_a$ and $\varphi_0 = -k/2,\ k = 2^\circ, 3^\circ, \ldots, 24^\circ$.

wavelength R and amplitude A, which is superimposed onto the background sound speed structure

$$\delta C(r,z) = A\frac{2z}{B}\,\mathrm{e}^{-2z/B}\sin\left(\frac{2\pi r}{R}\right). \tag{8}$$

Poincaré section. In a range dependent environment the ray trajectories partition a three dimensional (3D) extended phase space. (The 2D phases space is extended by the dimension of the independent variable, range.) It is convenient to reduce the dimension of the phase space of the dynamics while aiming to preserve all its important features. The standard way to do this for a periodic range dependency of the driving is to take the stroboscopic Poincaré sections of ray trajectories. In doing so, the phase space is bounded by considering only the modulus of the range coordinate with respect to the wavelength, $r_{mod} = \mathrm{mod}(r, R)$. This phase space can be viewed as cylindrical. The surface of intersection is chosen as a surface at constant range. The subsequent intersecting points being linked by segments of ray trajectories, and therefore the following mapping can be established for their connection:

$$(z_{n+1}, p_{n+1}) = \mathscr{P}(z_n, p_n), \quad \mathscr{P} = (\mathscr{P}_z, \mathscr{P}_p). \tag{9}$$

In Eq. (9) $\mathscr{P}$ is referred to as the Poincaré return map [7], and the Poincaré sections can be understood as plots of its trajectories. Fig. 2 shows the Poincaré sections of 23 ray trajectories of the perturbed ray system.

The Poincaré return map is one means of studying ray stability graphically. It can be shown that the Poincaré return map of a Hamiltonian system inherits the area preserving property of the flow, and is, therefore, an area preserving mapping. Consequently, the Jacobi determinant for the map is unity

$$\partial_z\mathscr{P}_z\partial_p\mathscr{P}_p - \partial_p\mathscr{P}_z\partial_z\mathscr{P}_p = 1. \tag{10}$$

The type of trajectory motion, chaotic or regular, can be identified by constructing a Poincaré section [10]. Where there are closed loops, called invariant curves as in Fig. 2, the motion is regular. Points filling a finite area correspond to chaotic trajectories. Motion of the former type has one constant, while motion of the latter type has none. That is, there are not enough constants in either case to render the ray system integrable. It is noted that the phase space is partitioned into nonintersecting regular and chaotic regions, as is predicted by the KAM-theory [10].

One feature to highlight here is the five-fold island structure in connection with a nonlinear (primary) resonance. The Poincaré sections of resonant trajectories are constituted by a finite number of points (fixed points of the motion), which are located at the centre of the islands. In such cases the two frequencies of the motion are commensurable, i.e the winding number is rational (in our example being 5:1). Secondary resonance is prompted by the island structure around each island of the primary resonance [10].

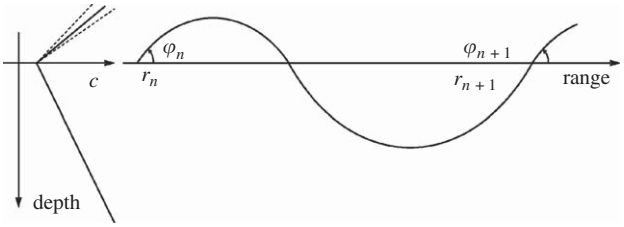

Fig. 3. A propagation scenario for the ocean model with the bilinear profile. The envelope of the perturbed profile is indicated by dashed lines.

An alternative map. In Ref. [4] a model with a bilinear sound speed profile was studied in which for convenience the zero of the depth coordinate was set at the channel axis. To model perturbation, the sound speed gradient above the channel axis is a periodic function of range which results in the following potential for the Hamiltonian:

$$V(r,z)=\begin{cases} gz(1+(\varepsilon/2)\cos(kr)), & z>0,\\ -hz, & z<0. \end{cases}$$

For such a simple model, analytical solutions can be found for ray paths above and below the channel axis and from these the authors derived an area preserving return map:

$$\rho_{n+1}=\rho_n+\phi_n+\gamma\phi_{n+1}+\varepsilon\sin(\rho_n), \tag{11}$$

$$\phi_{n+1}=\phi_n+\varepsilon[\sin(\rho_n)+\sin(\rho_n+\phi_n+\varepsilon\sin(\rho_n))]. \tag{12}$$

Here, $\gamma=g/h$, $\rho_n=kr_n$ and $\phi_n=2k\varphi_n/g$, where φ_n's are the positive ray angles at the channel axis separated by one ray cycle, and r_n is the corresponding range. (See Fig. 3.) From the construction of the model, it follows that the surface of intersection is at the channel axis. Only the upward refracted ray paths are considered (hence the return map). The choice of such a surface of intersection to reduce dimensionality is one alternative to the stroboscopic Poincaré section.

With general models of the sound speed profile when the resulting ray system is non-integrable, the map associated with a surface of intersection at the axis depth cannot be obtained analytically. Yet they exist, and we can treat them symbolically, i.e.,

$$(r_{n+1},p_{n+1})=\mathscr{M}^*(r_n,p_n),\quad \mathscr{M}^*=(\mathscr{M}^*_r,\mathscr{M}^*_p). \tag{13}$$

This alternative map can also be presented graphically. Note, however, that the evolution parameter, range, is monotonically increasing at subsequent intersections, and it is desirable when plotting to compress the range. For this purpose the range modulo the wavelength of the range variation is used and the trajectories of a modified map $\mathscr{M}$ are plotted. This is shown for the example in Fig. 4. This map preserves all important features of the Poincaré return map. Invariant curves indicate regular motion; the invariant curves and the area filling sections of chaotic ray trajectories belong to nonintersecting regions in the space of $\mathscr{M}$; resonant trajectories are associated with fixed points of $\mathscr{M}$.

4. Other reduction techniques

The existence of the two maps discussed above, $\mathscr{P}$ and $\mathscr{M}$, relies on the fact that for a periodic perturbation it is possible to make the 3D phase space cylindrical and so bounded. In any other case, i.e. non-periodic driving or no driving at all, these maps are not uniquely defined. Only $\mathscr{M}^*$ is well defined, but there is no obvious way to compress the range variation and so it does not support graphical studies.

For an ocean model with no variation of sound speed with range, the ray trajectories give a unique partition of the ray tangent-depth phase space. Hence the dynamics can be conveniently studied by the 2D phase portrait. Fig. 5 shows ray trajectories which sample the phase portrait for a Munk profile. It is possible to reduce the dynamics using intersections with a surface in two ways. The surface of intersection is again at the

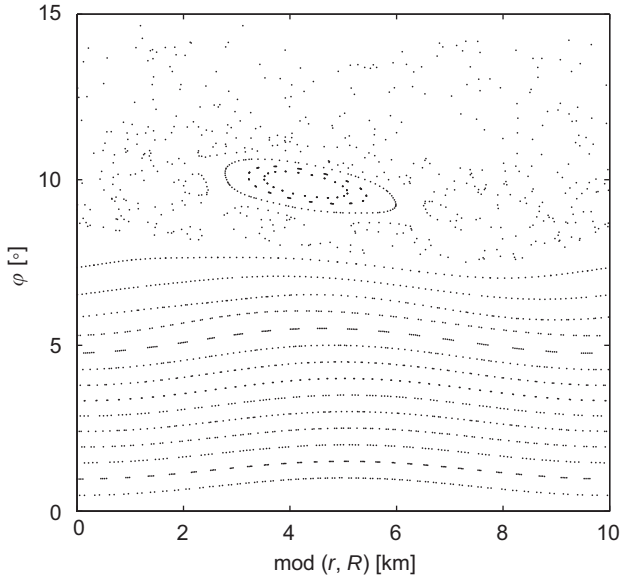

Fig. 4. An alternative to the Poincaré section of the ray trajectories. Parameters of single mode perturbation are: $A = 0.01$ and $R = 10$ km. Initial conditions are: $z_0 = z_a$ and $\varphi_0 = -k/2$, $k = 2^\circ, 3^\circ, \ldots, 24^\circ$.

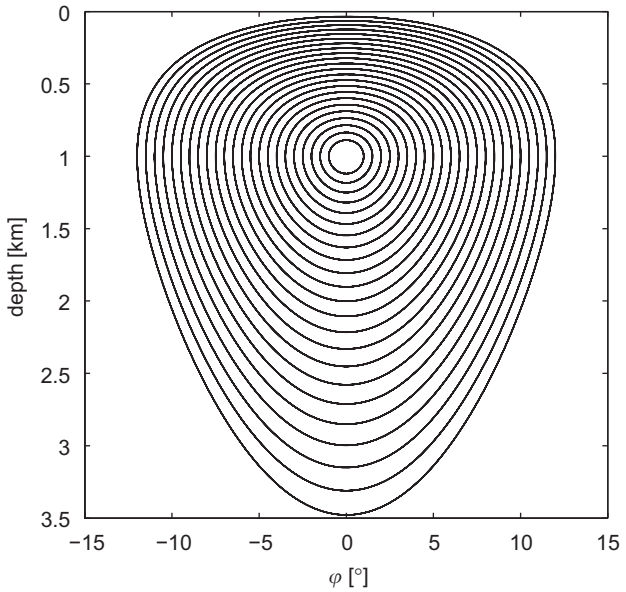

Fig. 5. Ray trajectories without perturbation. Initial conditions are: $z_0 = z_a$ and $\varphi_0 = -k/2$, $k = 2^\circ, 3^\circ, \ldots, 24^\circ$.

channel axis, but both positive and negative going ray intersections are allowed. Note that the ray tangent p_n may be either positive or negative; the range r_n is monotonically increasing.

The representation implied by the first reduction technique is a plot of the ray tangent, p_n, the value at the current intersection against the difference between this value and the one at the previous intersection, $p_n - p_{n-1}$. The representation implied by the second reduction technique is a plot of p_n, against the difference between the corresponding range and the one at the previous intersection, $r_n - r_{n-1}$. Fig. 6 shows the representations of the unperturbed ray system with both reduction techniques. Note that, as mentioned

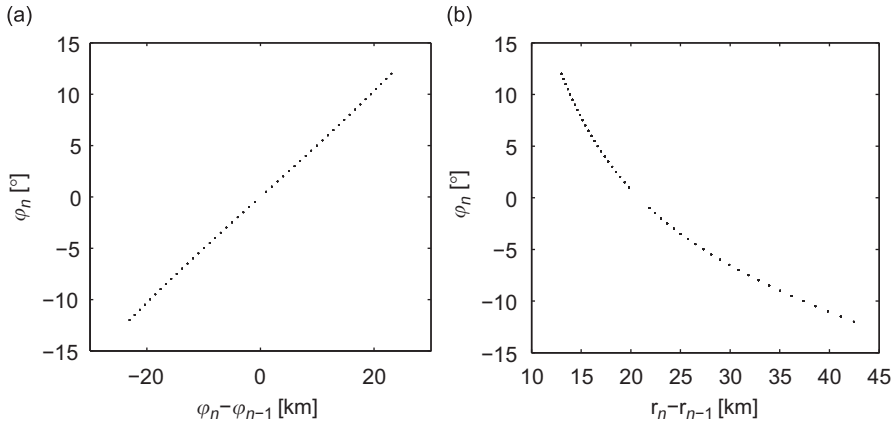

Fig. 6. Two representations of the unperturbed ray system: (a) the ray angle plotted against the difference in ray angle between subsequent intersections and (b) the ray angle plotted against the difference in range between subsequent intersections. Initial conditions are: $z_0 = z_a$ and $\varphi_0 = -k/2$, $k = 2°, 3°, \ldots, 24°$.

earlier, we plot a more intuitive variable φ, the ray angle, instead of the ray tangent p. With the first reduction technique, which ignores range (Fig. 6a), information can be extracted from the phase portrait (Fig. 5). The points lie on a straight line with a gradient of 0.5. This is due to the symmetry of the phase portrait ($p_n = -p_{n-1}$), so that $p_n - p_{n-1} = -2p_{n-1} = 2p_n$, and also $p_n/(p_n - p_{n-1}) = \frac{1}{2}$. Using the second reduction technique, involving range values as well (Fig. 6b), information can be provided about the lengths of the upper and lower loops of the ray paths: they are monotonic smooth functions of the ray take-off angles.

We now apply these techniques to the harmonically driven ray system. The results are shown in Fig. 7. Note that values are taken only at every other intersection, i.e. the plots are of p_{2n} against either $p_{2n} - p_{2n-1}$ or $r_{2n} - r_{2n-1}$. These representations preserve two features of $\mathscr{P}$ and $\mathscr{M}$. Closed loops and area filling points, respectively, indicate regular and chaotic motion; and resonant trajectories are associated with a finite number of points in the centre of islands. Both primary and secondary resonances are visible. The third feature of nonintersecting regular and chaotic regions does not apply. Closed loops may intersect other loops or the area filled by points due to chaotic motion. That is, coordinates need not belong to one trajectory uniquely, and so there are no associated maps.

It is worth noting that the loops and area filling points in Figs. 7a and b are confined by envelopes. The envelopes lie along curves already seen in Fig. 6, and their width clearly depend on the perturbation strength.

A third representation, shown in Fig. 8, is to plot the differences of successive ray tangents against the differences of the corresponding ranges, at every other intersection, i.e. $p_{2n} - p_{2n-1} = \Delta p_n$ against $r_{2n} - r_{2n-1} = \Delta r_n$. This plot preserves the main features seen in Fig. 7b; however, the range on the vertical axis has been doubled due to taking differences of successive tangents. Another difference is that loops are replaced with simple curve segments, and no curve segment overlaps any other nor does it merge into the chaotic sea; i.e. the space associated with this representation is partitioned into nonintersecting regular and chaotic regions.

5. Quasiperiodic driving

If there are two or more internal waves whose periods are incommensurable, the driving is said to be quasiperiodic. Although, it is periodic with the period which is the smaller of the smallest common multiple or the largest common divisor of all the periods involved. For higher mode numbers this period can be very large, so that the application of maps $\mathscr{P}$ and $\mathscr{M}$ is not feasible. It is often the case for $N = 2$ already. Therefore, such systems need different treatment.

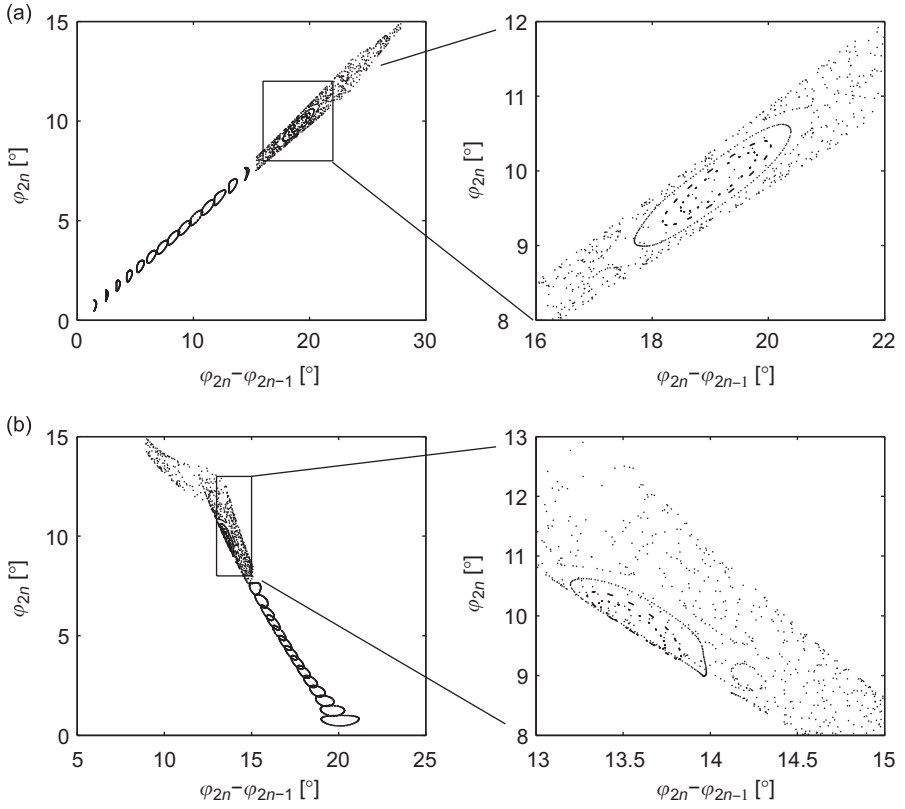

Fig. 7. Two representations of the unperturbed ray system: (a) the ray angle plotted against the difference in ray angle between subsequent intersections and (b) the ray angle plotted against the difference in range between subsequent intersections. Initial conditions are: $z_0 = z_a$ and $\varphi_0 = -k/2$, $k = 2^\circ, 3^\circ, \ldots, 24^\circ$. Blow-ups of figures on the left are displayed on their right.

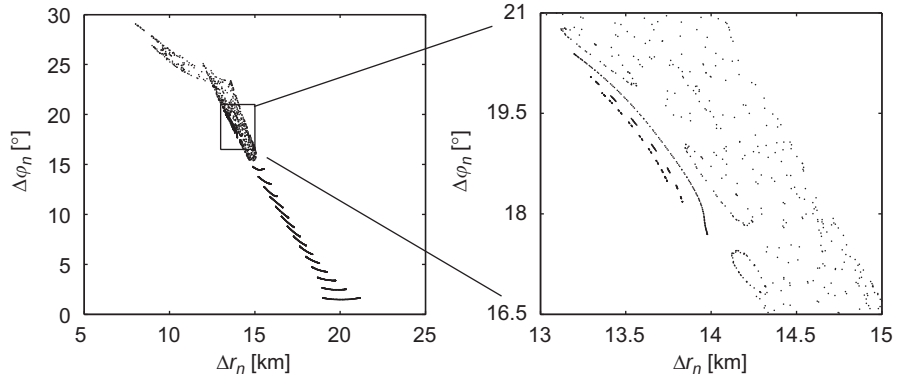

Fig. 8. A further representation of the perturbed ray system. Initial conditions are: $z_0 = z_a$ and $\varphi_0 = -k/2$, $k = 2^\circ, 3^\circ, \ldots, 24^\circ$.

For simplicity, consider just two waves, and let the second mode have the same depth variation as the first mode but with wavelength R_2 and a phase shift r_φ, so that

$$\delta C(r,z) = \frac{2z}{B}\,\mathrm{e}^{-2z/B}\left[A_1 \sin\left(\frac{2\pi r}{R_1}\right) + A_2 \sin\left(\frac{2\pi(r+r_\varphi)}{R_2}\right)\right]. \tag{14}$$

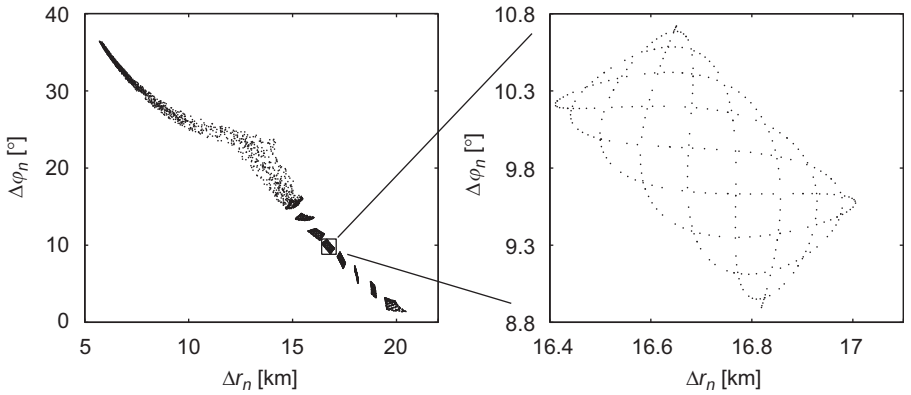

Fig. 9. The representation of the ray system with a two mode perturbation model applying the third graphical technique. The perturbation parameters are: $A_1 = A_2 = 0.01$, $R_1 = 7\,\text{km}$, $R_2 = 13\,\text{km}$, $r_\varphi = 5\,\text{km}$. Initial conditions are: $z_0 = z_a$ and $\varphi_0 = -1^\circ, -2^\circ, \ldots, -12^\circ$. The curve with $\varphi_0 = -5^\circ$ is magnified.

Fig. 9 shows the representation of the ray dynamics using the last reduction technique introduced above. Regular and chaotic motions are, respectively, indicated by either curves similar to the Lisajous curves or area filling points. The curves of regular motion intersect either other such curves or merge into the chaotic sea, therefore, the property of nonintersecting regular and chaotic partition of the space associated with the representation does not hold with quasiperiodic driving. The blown-up curve in Fig. 9, which is similar to a Lisajous curve, is not closed.

6. Summary and discussion

For sufficiently small perturbation a fraction of the Poincaré sections of periodically perturbed ray trajectories are regular, and the region that they belong to is immersed into a chaotic sea in phase space (Fig. 2). This is consistent with predictions of the KAM-theory. We have seen that other representations of the dynamics, those associated with map $\mathscr{M}$ and the third one of the newly introduced reduction techniques, provide graphical means for drawing the same conclusion.

More realistic models of the perturbation involve a sum of N range-periodic internal-wave modes. Most generally the corresponding Hamiltonian is assumed to have quasiperiodic range dependency, which means that the internal-wave lengths are allowed to be incommensurate. It was shown in Ref. [2] that for such systems the KAM-theory has implications similar to those cited above for systems with a range-periodic Hamiltonian. The argument is based on the fact that systems of $N \geqslant 2$ can be transformed into an $N+1$ degrees-of-freedom autonomous system, whose phase space can be bounded by multiple use of the modulo function. (For details refer to Ref. [2].) For smaller N's it is feasible to illustrate the implications of the KAM-theory by viewing multiply sectioned trajectories. In practice, for $N = 2$, this means viewing trajectories at integer multiples of R_1, then, plotting those points in the ray tangent-depth plane which satisfy the inequality $|\text{mod}(r, R_2) - r_0| < \delta$. Here, r_0 is an arbitrary constant between 0 and R_2, and δ controls the accuracy of the numerical procedure. Such multiply sectioned trajectories for the ray system with the quasiperiodic perturbation introduced in the previous section, similar to those in the referenced paper, are displayed in Fig. 10.

Given a certain range of simulation, the number of points to plot is increasing with increasing δ. The accuracy, however, whether these points in phase space are close to the sectioning surface is decreasing. In contrast, with the approach presented above, the points which constitute a curve like the one magnified in Fig. 9 lie on the surface of intersection at the axis depth to within the accuracy of a root-finding procedure, and the range of simulation determines solely the number of points to plot. Furthermore, Fig. 9 supports the idea of nonintersecting regular and chaotic regions in the phase space of the ray equations, i.e. a dense set of stable solutions (readily demonstrated in Fig. 10). Note the cascade of sections of regular orbits.

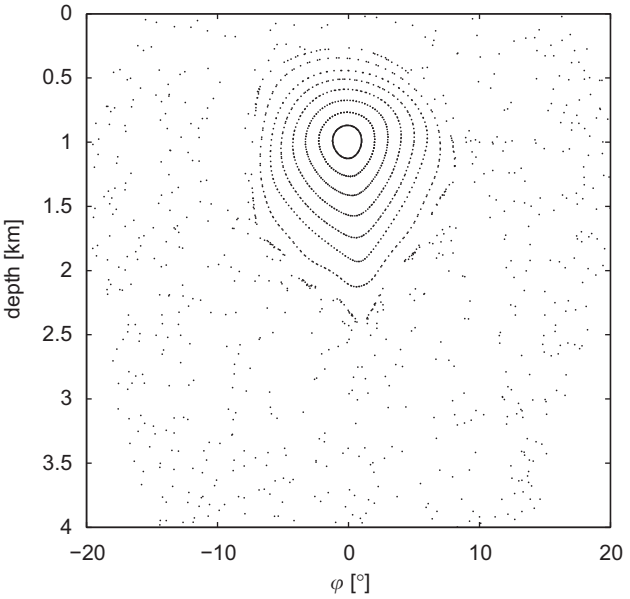

Fig. 10. Multiply sectioned trajectories. Initial conditions are: $z_0 = z_a$ and $\varphi_0 = 1^\circ, \ldots, 12^\circ$.

It is pointed out that increasing N implies higher dimensionality of the problem. In Ref. [2] it was associated with the higher $(2(N+1))$ dimensional phase space of the equivalent autonomous system. Here it is manifested by the following. We consider plots of the representations associated with the third reduction technique introduced above in the case of $N = 0$, 1, 2. With no perturbation ($N = 0$), sectioning the trajectories results in single points; with harmonic perturbation ($N = 1$) the sections of regular trajectories are (nonintersecting) curve segments. In case of the simplest quasiperiodic perturbation ($N = 2$) the increasing dimensionality is indicated by the intersecting sections of regular trajectories (Fig. 9).

Acknowledgements

MW and TB wishes to thank the College of Physical Sciences of the University of Aberdeen for the financial support. The support of the Royal Academy of Engineering given to AJF during his secondment to the University as an industry to academia fellow is gratefully acknowledged.

References

[1] F.J. Beron-Vera, M.G. Brown, J.A. Colosi, S. Tomsovic, A.L. Virovlyansky, M.A. Wolfson, G.M. Zaslavsky, Ray dynamics in a long-range acoustic propagation experiment, *Journal of the Acoustical Society of America* 114 (3) (2003) 1226–1242.
[2] M.G. Brown, Phase space structure and fractal trajectories in 11/2 degree of freedom hamiltonian systems whose time dependence is quasiperiodic, *Nonlinear Processes in Geophysics* 5 (2) (1998) 69–74.
[3] M.G. Brown, J.A. Colosi, S. Tomsovic, A.L. Virovlyansky, M.A. Wolfson, G.M. Zaslavsky, Ray dynamics in long-range deep ocean sound propagation, *Journal of the Acoustical Society of America* 113 (5) (2003) 2533–2547.
[4] M.G. Brown, F.D. Tappert, G. Goni, An investigation of sound ray dynamics in the ocean volume using an area preserving mapping, *Wave Motion* 14 (1991) 93–99.
[5] J.A. Colosi, M.G. Brown, Efficient numerical simulation of stochastic internal-wave-induced sound-speed perturbation fields, *Journal of the Acoustical Society of America* 103 (4) (1998) 2232–2235.
[6] C. Garrett, W.H. Munk, Space-time scales of internal waves, *Geophysical and Astrophysical Fluid Dynamics* 3 (1) (1972) 225.
[7] J. Guckenheimer, P. Holmes, *Nonlinear Oscillations, Dynamical Systems and Bifurcations of Vector Fields*, Springer, New York, 1983.
[8] R.H. Hardin, F.D. Tappert, Applications of the split-step Fourier method to the numerical solution of nonlinear and variable coefficient wave equations, *SIAM Review* 15 (1973) 423.
[9] F.B. Jensen, W.A. Kuperman, M.B. Porter, H. Schmidt, *Computational Ocean Acoustics*, Springer, New York, 2000.

[10] A.J. Lichtenberg, M.A. Lieberman, *Regular and Stochastic Motion*, Springer, New York, 1982.
[11] W.H. Munk, Sound channel in an exponentially stratified ocean, with application to SOFAR, *The Journal of the Acoustical Society of America* 55 (2) (1974) 220–226.
[12] D.R. Palmer, M.G. Brown, F.D. Tappert, H.F. Bezdek, Classical chaos in nonseparable wave propagation problems, *Geophysical Research Letters* 15 (6) (1988) 569–572.
[13] I.P. Smirnov, A.L. Virovlyansky, G.M. Zaslavsky, Theory and applications of ray chaos to underwater acoustics, *Physical Review E* 64 (3) (2001) 036221.
[14] I.P. Smirnov, A.L. Virovlyansky, G.M. Zaslavsky, Sensitivity of ray travel times, *Chaos* 12 (3) (2002) 617–635.
[15] I.P. Smirnov, A.L. Virovlyansky, G.M. Zaslavsky, Ray chaos, travel time modulation, and sensitivity to the initial conditions, *Journal of the Acoustical Society of America* 117 (3) (2005) 1595–1606.
[16] F.D. Tappert, The parabolic approximation method, *Wave Propagation and Underwater Acoustics*, vol. 70, Springer, Berlin, Heidelberg, 1977, pp. 224–287 (Chapter 5).
[17] M. Wiercigroch, A.H.-D. Cheng, J. Simmen, M. Badiey, Nonlinear behavior of acoustic rays in underwater sound channels, *Chaos, Solitons, & Fractals* 9 (1–2) (1998) 193–207.